Phase-Field Crystal Modeling of Compositional Domain Formation in Ultrathin Films

Srevatsan Muralidharan*
Department of Mechanical and Aerospace Engineering, Princeton University, Princeton, New Jersey 08544, USA

Mikko Haataja†
Department of Mechanical and Aerospace Engineering, Princeton Institute for the Science and Technology of Materials (PRISM), and Program in Applied and Computational Mathematics (PACM), Princeton University, Princeton, New Jersey 08544, USA
(Received 22 June 2010; published 17 September 2010)

Bulk-immiscible binary systems often form stress-induced miscible alloy phases when deposited on a substrate. Both alloying and surface dislocation formation lead to the decrease of the elastic strain energy, and the competition between these two strain-relaxation mechanisms gives rise to the emergence of pseudomorphic compositional nanoscale domains, often coexisting with a partially coherent single phase. In this work, we develop a phase-field crystal model for compositional patterning in monolayer aggregates of binary metallic systems. We first demonstrate that the model naturally incorporates the competition between alloying and misfit dislocations, and quantify the effects of misfit and line tension on equilibrium domain size. Then, we quantitatively relate the parameters of the phase-field crystal model to a specific system, CoAg/Ru(0001), and demonstrate that the simulations capture experimentally observed morphologies.

DOI: 10.1103/PhysRevLett.105.126101 PACS numbers: 68.35.Md, 68.35.Dv

It is well known that materials confined in one or more dimensions may display properties (chemical, physical, electronic, and mechanical) which can be strikingly different from those of the corresponding bulk materials. Illustrative examples are provided by binary metallic systems, such as CuAg on Ru [1], PdAu on Ru [2], and CoAg on Ru [3], which are immiscible in the bulk and yet form miscible phases with typical compositional domain size $\sim$3 nm when deposited on a substrate as a (sub)monolayer aggregate. In this case, the mixing of the two components is brought upon by the epitaxial nature of the growth processes, whereby the surface alloy phase adopts the lattice spacing of the substrate; the pure components would be subjected to substantial misfit strains relative to the substrate. For example, in the CoAg/Ru(0001) system, where the misfit strains are $\sim \pm 8\%$, it has been experimentally observed that for Ag-rich compositions, the alloy either displays a single mixed phase, or two coexisting phases; in the latter case, the alloy phase remains fully coherent with the substrate while the other is only partially coherent, with dislocations relaxing the misfit strains [3,4].

Theoretically, the formation of alloys in such films can be understood by considering the reduction in elastic energy of the system brought upon by mixing [1,3–9]. Atomistically detailed models for alloy formation energies have led to impressive agreement with experimental and theoretical phase diagrams for surface-constrained alloys for a few specific systems [3,6,7,9], and kinetic Monte Carlo simulations of the formation dynamics of compositional domains with interaction parameters determined from *ab initio* calculations have been carried out recently [9,10]. Inherent in these simulations, however, is the assumption that the ultrathin film remains pseudomorphic with the underlying substrate, and strain relaxation via misfit dislocation formation is not allowed; such limitations restrict the range of compositions that can be investigated with regard to domain formation kinetics.

In light of the discussion above, it is clear that a quantitative approach to compositional patterning at the nanoscale necessarily must incorporate alloy (bulk) thermodynamics, the presence of elastic strains and misfit dislocations within the surface layer, and diffusive kinetics of the alloy components on the surface. In this Letter, we present an approach based on the so-called phase-field crystal (PFC) method [11–15] for compositional patterning in ultrathin films. We first demonstrate that the model naturally incorporates the competition between alloying and misfit dislocation formation, and quantify the effects of misfit and line tension on equilibrium domain size. Then, we relate the parameters of the PFC model to a specific system, CoAg/Ru(0001), and demonstrate that the simulations capture experimentally observed morphologies.

Model equations.—The free-energy functional used in this work is written as

$$F[\rho, C] = \int \Bigg[\Bigg(\frac{\rho}{2}\{r(c) + [q(c)^2 + \nabla^2]^2\}\rho + \frac{\rho^4}{4} \Bigg) + V(c)\rho + f_0 \Bigg\{ \frac{w_0^2}{2}(\nabla c)^2 - \frac{\theta_c}{2}c^2 + \frac{\theta}{2}[(1+c) \times \log(1+c) + (1-c)\log(1-c)] \Bigg\} \Bigg] d\mathbf{r}, \tag{1}$$

where $\rho(\mathbf{r}, t)$ is the atomic density field, $c(\mathbf{r}, t)$ denotes the concentration field (with fixed spatial average $\bar{c}$ and $c = \pm 1$ representing different atomic species), $V(c)$

 © 2010 The American Physical Society

denotes the (species-specific) substrate-film interaction energy, $q(c) = 1 - \epsilon c/2 + \epsilon^2 c^2/4$ incorporates the bulk lattice constants of different species, f_0 dictates the relative importance of elastic and chemical energies, θ_c is the critical temperature above which there is no phase-separation, θ is the system temperature, and $w_0 > 0$ contributes to interfacial energy between different species. Furthermore, the linear function $r(c) = A_r + B_r c$ is employed to tune the elastic properties of the adlayer, as will be discussed later. Note that in Eq. (1), the first term incorporates elastic and plastic deformation energies of the depositing atoms, the second term models the interaction between the substrate and the depositing atoms [16], while the third term accounts for the bulk thermodynamics of the binary system within simple regular solution theory. We treat the substrate as rigid, and thus do not incorporate long-ranged dipolar interactions between the domains mediated by the substrate [6,17–19]; as discussed in Ref. [9], these interactions are not expected to dominate the aggregate structure at the nanoscale. The dynamics of ρ and c are conserved, and hence the variational evolution equations are given by $\partial\rho/\partial t = M_\rho \nabla^2(\delta F/\delta\rho)$ and $\partial c/\partial t = M_c \nabla^2(\delta F/\delta c)$. In order to eliminate unphysical spatial variations in $c(\mathbf{r}, t)$ within a single atom, we impose the condition $\hat{c}(\mathbf{k}, t) = 0$ for $k^2 > k_f^2$, where k_f denotes a cutoff wave number to be specified below, and $\hat{c}$ denotes the Fourier transform of $c(\mathbf{r}, t)$. We also expand the logarithmic free energy in Eq. (1) in powers of c up to c^{52} in order to impose the condition $|c(\mathbf{r}, t)| \leq 1$.

For the film-substrate potential, we employ a simple form [20], which allows us to conveniently tune the species-specific interaction energy of an adatom on the substrate hcp, fcc, or bridge sites: $V(c) = -V_a(c)\sum_j \cos(\mathbf{K}_j \cdot \mathbf{r}) + V_b(c)\sum_j \sin(\mathbf{K}_j \cdot \mathbf{r})$. Here, $\mathbf{K}_j$ denote the reciprocal lattice vectors of the hexagonal lattice, while $V_i = A_i + B_i c$ for $i = a$ or b. In order to highlight the relevant physics, we will first consider the scenario where only one site (either fcc or hcp) has a much more favorable interaction energy compared to other substrate sites; this can be achieved by setting, say, $A_a = B_a = B_b = 0$ and $A_b = -V_0$. Later, we will relax this assumption when discussing a specific system [CoAg on Ru(0001)].

Analytical arguments.—To get a better understanding of the physics incorporated in Eq. (1), we first analyze the problem in 1D. When the misfit $\delta(x) = \epsilon c(x)/2$ between the depositing and substrate atoms is small, the energy minimizing density field within a single-mode approximation takes the form $\hat{\psi} = \bar{\psi} + Ae^{ix+i\phi(x)} + \text{c.c.}$, where "c.c." denotes complex conjugation. Upon assuming a fixed compositional variation $c(x)$, setting $A = \text{const}$, writing $V(x) = V_0(e^{ix} + e^{-ix})$, and substituting the expression for $\hat{\psi}$ in Eq. (1) and neglecting $O(\delta^3)$ terms and higher, we obtain $F = \int\{4A^2[\frac{d\phi(x)}{dx} + \delta(x)]^2 - 2AV_0\cos[\phi(x)]\}dx$, which is the continuum version of the celebrated Frenkel-Kontorowa (FK) model [8,21] with a spatially varying misfit. In the case of a compositional lamellar phase of width L_c at $\bar{c} = 0$, one finds that the energy density of a pseudomorphic phase [for which $\phi(x) \ll 1$] becomes

$$E_{\text{tot}}/L_c = \left\{A^2\epsilon^2\left[1 - \frac{2}{\xi L_c}\tanh\left(\frac{\xi L_c}{2}\right)\right] + \frac{\Gamma}{L_c}\right\}, \qquad (2)$$

where $\xi^2 = V_0/(4A)$ is the inverse decay length of elastic deformations away from compositional interfaces, and $\Gamma = 2\sqrt{2}f_0 w_0/3$ denotes the line tension arising from chemical interactions. Further, to account for important 2D effects, such as longitudinal elastic strains along compositional interfaces, we replace the parameters Γ, V, and A with effective ones (Γ_{eff}, V_{eff}, and A_{eff}), extracted via linearization of the concentration equation in the pseudomorphic limit in both 1D and 2D, and compare the resulting expressions [22]. On minimization, Eq. (2) shows that coarsening will not take place when $\Gamma_{\text{eff}} < \Gamma^*_{\text{eff}} \equiv 2A^2_{\text{eff}}\epsilon^2/\xi_{\text{eff}}$. Furthermore, when $\Gamma_{\text{eff}} \ll \Gamma^*_{\text{eff}}$ and

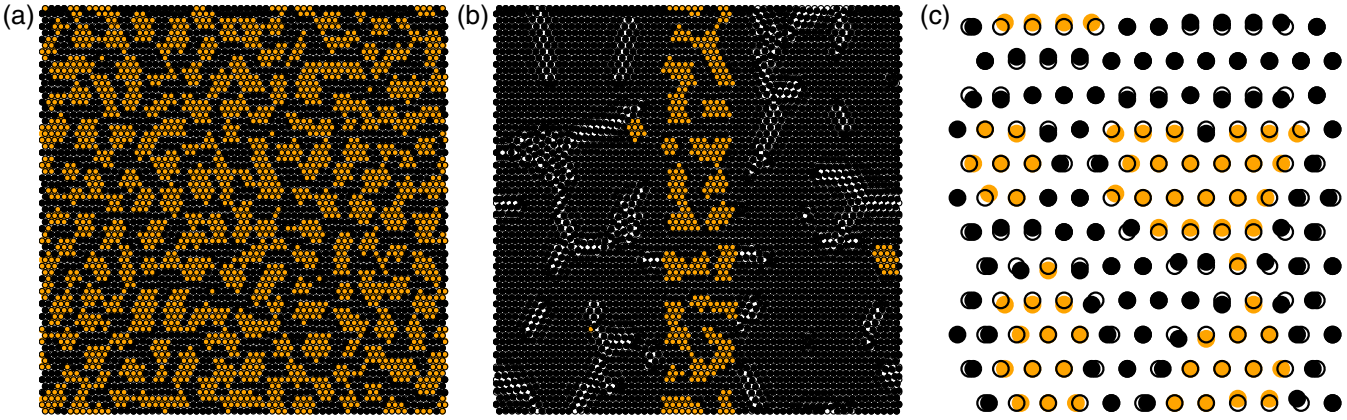

FIG. 1 (color online). Results from PFC simulations. Filled dark (light) circles represent atoms of type A (B). Panel (a) shows the formation of nanodomains for the 50-50 alloy ($\bar{c} = 0$). Panel (b) reveals the coexistence between a pure, dislocated majority phase and a pseudomorphic alloy phase for $\bar{c} = 0.75$. Incommensurate regions appear as white strings in this figure. Panel (c) is a magnification of the 50-50 alloy, which reveals significant elastic relaxation of the atoms away from the local potential energy minima (indicated by open circles) in the vicinity of interfaces.

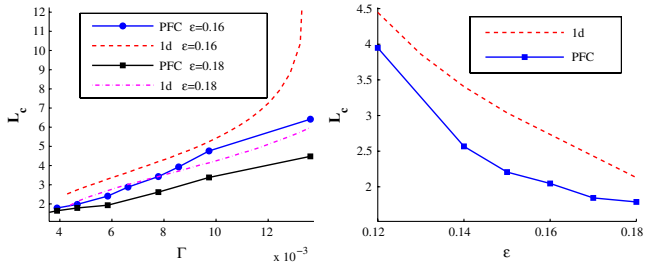

FIG. 2 (color online). Domain sizes in units of the substrate lattice spacing at varying line tension Γ (left panel) and misfit ϵ (right panel). The dashed lines are parameter-free predictions based on Eq. (2).

$L_c^* \xi_{\rm eff} \ll 1$, $L_c^* \sim (\Gamma_{\rm eff}/A_{\rm eff}^2 \epsilon^2 \xi_{\rm eff}^2)^{1/3}$. These predictions, together with numerical minimization of Eq. (2), will be compared against full simulations of the PFC model below.

Numerical implementation.—We carry out numerical simulations on a 512×512 uniform lattice with grid spacing $\Delta x = \pi/4$, $\Delta y = \pi/(2\sqrt{3})$, and time step $\Delta t = 0.5$ with representative parameter values $A_r = -0.7$, $B_r = 0$, $\bar{\rho} = 0.32$, $\epsilon = 0.18$, $V_0 = 0.015$, $f_0 = 0.005$, $k_f^2 = 0.7$, $w_0 = 2\pi/\sqrt{3}$, $\theta_c = 6$, and $\theta = 3$. The readers are referred to Refs. [23,24] for details regarding the numerical method. To facilitate visualization of the configurations, we first extract the local maxima from $\rho(\mathbf{r}, t)$ and assign equivalent particle positions to these maxima [25], and then plot the particles. Representative steady state configurations attained for the parameters values at $\bar{c} = 0$ and $\bar{c} = 0.75$ are shown in Figs. 1(a) and 1(b), respectively, while Fig. 1(c) shows a magnified view of the atomic positions near compositional domain walls. As expected, nanodomains emerge from small initial fluctuations in $c(\mathbf{r}, 0)$ due to strain relaxation in the $\bar{c} = 0$ case. Interestingly, Fig. 1(b) reveals the coexistence between a commensurate alloy phase and dislocated majority phase that emerges from a stripe initial condition corresponding to $c(\mathbf{r}, 0) = 0$ within the stripe and $c(\mathbf{r}, 0) > 0$ outside, in qualitative agreement with experimental observations in Ref. [3]. Finally, note the significant relaxation of the atoms away from the substrate potential minima along the compositional interfaces in Fig. 1(c), also seen in experiments [4].

Turning now to a more quantitative analysis, we have performed several numerical simulations at $\bar{c} = 0$ and different ϵ and Γ values in order to extract the equilibrium domain size $L_c \equiv L^2/L_{\rm int}$, where $L_{\rm int}$ denotes the total interface length between the compositional domains. The data, displayed in Fig. 2, show that increasing line tension Γ leads to an increase in L_c, while increasing misfit ϵ will lead to a concomitant decrease in the domain size, as expected. Figure 2 also shows the direct comparison between the full PFC simulations and the continuum FK predictions for the domain size without any adjustable parameters. It can be seen that the FK results, while systematically overestimating the domain sizes, nevertheless capture the trends in the PFC data surprisingly well, given the approximations inherent in the analysis.

Quantitative modeling of CoAg *on* Ru(0001).—We next demonstrate how the model can be employed to simulate specific materials systems. We have chosen CoAg on Ru(0001) as the model system, since both first-principles and experimental data for the model parameters exist. First, we note that the adatom-substrate interaction energy per unit area in the PFC approach is given by $A_{\rm cell}^{-1} \int \rho V dA_{\rm cell}$, where $A_{\rm cell}$ denotes the area of the unit cell. Then, we employ a single-mode approximation $\rho(\mathbf{r}) = \bar{\rho} + A \sum_j e^{i\mathbf{K}_j \cdot \mathbf{r} + i\phi_j} + \text{c.c.}$, where the phases ϕ_j are chosen such that the adlayer atoms reside on top of the substrate bridge, fcc, or hcp sites, and carry out the integrations to yield $\frac{1}{2} A V_a + \frac{3\sqrt{3}}{2} A V_b = \frac{V_{\rm bridge} - V_{\rm hcp}}{(\sqrt{3} a_{\rm Ru}^2/2)}$ and $\frac{1}{2} A V_a - \frac{3\sqrt{3}}{2} A V_b = \frac{V_{\rm bridge} - V_{\rm fcc}}{(\sqrt{3} a_{\rm Ru}^2/2)}$. Here, $a_{\rm Ru} = 2.71$ Å [3], and $V_{\rm hcp} = 0$ by convention. Next, given $V_{\rm bridge}$ and $V_{\rm fcc}$,

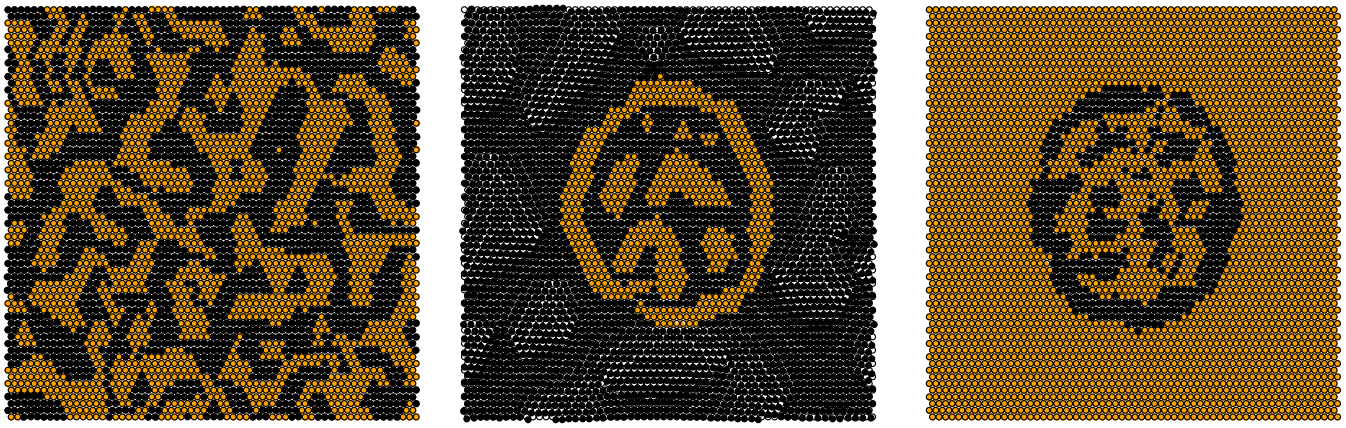

FIG. 3 (color online). Simulation results for CoAg/Ru(0001) system. Filled dark (light) circles represent Ag (Co) atoms, while the open circles represent hcp sites on Ru(0001). Left panel: pseudomorphic nanoscale alloy for $\bar{c} = 0$. Middle panel: in an Ag-rich system ($\bar{c} = 0.75$), a pseudomorphic alloy phase coexists with a partially commensurate pure Ag phase displaying stacking faults and dislocations. Right panel: in a Co-rich system ($\bar{c} = -0.75$), a pseudomorphic alloy phase coexists with a pseudomorphic Co phase.

we can solve for V_a and V_b in terms of amplitude A, while A in turn is related to the spring constant K via $K = 4\sqrt{3}A^2$, as can be verified by taking the continuum limit of the discrete FK model for a single-component system. Finally, given the target amplitudes A for Ag and Co, $r(c)$ is determined via an energy minimization calculation within the single-mode approximation.

For the CoAg/Ru(0001) system, we employ the *ab initio* values $K^{\mathrm{Co}} = 1300$ meV/Å^2, $V^{\mathrm{Co}}_{\mathrm{bridge}} = 220$ meV, $K^{\mathrm{Ag}} = 3800$ meV/Å^2, and $V^{\mathrm{Ag}}_{\mathrm{bridge}} = 50$ meV from Ref. [4], $V^{\mathrm{Co}}_{\mathrm{fcc}} = 132$ meV and $V^{\mathrm{Ag}}_{\mathrm{fcc}} = 4$ meV [26], and experimentally measured misfits of $+8\%(-7\%)$ for Ag (Co) [3] to fit the PFC parameters [27]. Figure 3 illustrates representative morphologies obtained for three different average compositions $\bar{c}$. As observed in experiments [3], a pseudomorphic nanoscale alloy emerges in the symmetric case $\bar{c} = 0$ from small initial fluctuations in $c(\mathbf{r}, 0)$, wherein the adatoms occupy the hcp surface sites. The compositional domains are elongated with a typical width of $\sim$5 atoms. On the other hand, starting from an initial condition corresponding to a single droplet with $c(\mathbf{r}, 0) = 0$ embedded within a domain with $c(\mathbf{r}, 0) > 0$ (<0) for an Ag (Co)-rich system, the emerging morphology strongly depends on the average composition. In particular, for the Ag-rich system, we observe a coexistence between a pure Ag phase displaying stacking faults and dislocations, and a pseudomorphic alloy phase. Again, the alloy domains are elongated with a typical width of $\sim$4 atoms. Also, a more careful analysis of the morphology of pure Ag systems on Ru(0001) reveals [28] the emergence of regular herringbone structures, where the Ag atoms reside on top of the fcc substrate sites and corresponding dislocations are arranged in a periodic manner, in agreement with experimental observations [29]. In contrast, the Co-rich phase remains fully commensurate over the whole composition range, and coexists with the pseudomorphic alloy phase, also in agreement with experimental observations [3].

Discussion.—In summary, we have developed a quantitative phase-field crystal model for the study of compositional domain formation in ultrathin films. We demonstrated that for pseudomorphic films, the dependence of the equilibrium domain size on line tension and misfit is well captured by an effective one-dimensional model based on the Frenkel-Kontorowa model. Furthermore, upon matching the PFC parameters to *ab initio* data for the CoAg/Ru(0001) system, excellent correspondence between simulated and experimentally observed morphologies was found. In particular, in the case of Co-rich systems, both coexisting phases (alloy phase and pure Co phase) remain pseudomorphic, while in the case of Ag-rich systems, the pure Ag phase displays dislocations and stacking faults.

This work has been in part supported by NSF-DMR Grants No. DMR-0449184 and No. DMR-0819860. We would also like to thank Dr. Vidvuds Ozolins for providing the requisite *ab initio* data for the CoAg/Ru system.

*smuralid@princeton.edu
†mhaataja@princeton.edu

[1] J. L. Stevens and R. Q. Hwang, Phys. Rev. Lett. **74**, 2078 (1995).
[2] G. E. Thayer *et al.*, Mater. Res. Soc. Symp. Proc. **619**, 85 (2000).
[3] G. E. Thayer *et al.*, Phys. Rev. Lett. **86**, 660 (2001).
[4] G. E. Thayer *et al.*, Phys. Rev. Lett. **89**, 036101 (2002).
[5] J. Tersoff, Phys. Rev. Lett. **74**, 434 (1995).
[6] V. Ozolins, M. Asta, and J. J. Hoyt, Phys. Rev. Lett. **88**, 096101 (2002).
[7] B. D. Krack, V. Ozolins, M. Asta, and I. Daruka, Phys. Rev. Lett. **88**, 186101 (2002).
[8] I. Daruka and J. C. Hamilton, J. Phys. Condens. Matter **15**, 1827 (2003).
[9] B. Yang, T. Muppidi, V. Ozolins, and M. Asta, Phys. Rev. B **77**, 205408 (2008).
[10] B. Yang, T. Muppidi, V. Ozolins, and M. Asta, Surf. Sci. **602**, L123 (2008).
[11] K. R. Elder, M. Katakowski, M. Haataja, and M. Grant, Phys. Rev. Lett. **88**, 245701 (2002).
[12] K. R. Elder and M. Grant, Phys. Rev. E **70**, 051605 (2004).
[13] P. Stefanovic, M. Haataja, and N. Provatas, Phys. Rev. Lett. **96**, 225504 (2006).
[14] K. R. Elder *et al.*, Phys. Rev. B **75**, 064107 (2007).
[15] K. R. Elder, Z. F. Huang, and N. Provatas, Phys. Rev. E **81**, 011602 (2010).
[16] C. V. Achim *et al.*, Phys. Rev. E **74**, 021104 (2006).
[17] O. L. Alerhand, D. Vanderbilt, R. D. Meade, and J. D. Joannopoulos, Phys. Rev. Lett. **61**, 1973 (1988).
[18] K.-O. Ng and D. Vanderbilt, Phys. Rev. B **52**, 2177 (1995).
[19] V. Shchukin and D. Bimberg, Rev. Mod. Phys. **71**, 1125 (1999).
[20] S. Narasimhan and D. Vanderbilt, Phys. Rev. Lett. **69**, 1564 (1992).
[21] P. Bak, Rep. Prog. Phys. **45**, 587 (1982).
[22] This procedure leads to $A^2_{\mathrm{eff}} = 2A^2_{\mathrm{2D}}$, $V_{\mathrm{eff}} = 4\sqrt{2}V_{0;\mathrm{2D}}/3$, and $\Gamma_{\mathrm{eff}} = \frac{2\sqrt{2}}{3} f_{\mathrm{eff}} w_{0\mathrm{eff}}$, where $f_{\mathrm{eff}} = [f_{\mathrm{2D}}(\theta_c - \theta) - \frac{5}{2}\epsilon^2 \bar{\psi}^2 - 2A^2_{\mathrm{2D}}\epsilon^2]$ and $w_{0\mathrm{eff}} = w_{\mathrm{2D}}\sqrt{f_{\mathrm{2D}}/f_{\mathrm{eff}}}$.
[23] M. Cheng and J. A. Warren, J. Comput. Phys. **227**, 6241 (2008).
[24] J. Z. Zhu, L. Q. Chen, J. Shen, and V. Tikare, Phys. Rev. E **60**, 3564 (1999).
[25] Particle identities at maxima are fixed by $c > c^*$ ($<c^*$) representing A (B) atoms, where c^* is chosen such that the overall composition equals $\bar{c}$.
[26] V. Ozolins (private communication).
[27] The matching procedure leads to the following choices of the PFC parameter values: $V_a(1) = 0.007\,23$, $V_b(1) = -0.000\,05$, $V_a(-1) = 0.0352$, $V_b(-1) = -0.0028$, $r(1) = -0.6$, $r(-1) = -0.18$, and $\epsilon = 0.15$; these values uniquely fix the coefficients A_i and B_i, where $i = r$, a, or b. The other PFC parameters were set to $\bar{\rho} = 0.25$, $f_0 = 0.0023$, $\theta_c = 3$, $\theta = 1.5$, and $k_f^2 = 0.48$, which translate to a line tension of $\Gamma^{\mathrm{chemical}}_{\mathrm{eff}} = 264$ meV/atom, obtained from the energy per boundary atom E^b via $E^b = \Gamma^{\mathrm{chemical}}_{\mathrm{eff}} K a_{\mathrm{Ru}}/(8\sqrt{3}A^2)$.
[28] S. Muralidharan, R. Khodadad, and M. Haataja (to be published).
[29] W. L. Ling *et al.*, Surf. Sci. **600**, 1735 (2006).